J Solid State Electrochem (2010) 14:1509–1513
DOI 10.1007/s10008-009-0970-7

ORIGINAL PAPER

Water-in-oil microemulsion method preparation and capacitance performance study of $Li_4Mn_5O_{12}$

Yan Zhao · Xiaoyun Xu · Qiongyu Lai · Yanjing Hao · Ling Wang · Zhien Lin

Received: 29 September 2009 / Revised: 30 October 2009 / Accepted: 2 November 2009 / Published online: 24 November 2009

Abstract Spinel $Li_4Mn_5O_{12}$ nanoparticles are successfully prepared by water-in-oil microemulsion method and characterized by X-ray diffraction and scanning electron microscopy. The $Li_4Mn_5O_{12}$ nanoparticles have sphere-like morphology with particle size less than 50 nm. The $Li_4Mn_5O_{12}$ and activated carbon (AC) were used as electrodes of $Li_4Mn_5O_{12}$/AC supercapacitor, respectively. The electrochemical capacitance performance of the supercapacitor was investigated by cyclic voltammetry, galvanostatic charge/discharge, and electrochemical impedance spectroscopy. The results showed that the single electrode was able to deliver specific capacitance 252 F g^{-1} within potential range 0–1.4 V at a scan rate of 5 mV s^{-1} in 1 mol L^{-1} Li_2SO_4 solution, and it also showed high coulombic efficiency close to 100%. This material exhibited a good cycling performance.

Keywords $Li_4Mn_5O_{12}$ · Microemulsion · Nanoparticle · Electrode material · Capacitance performance

Introduction

Supercapacitors have attracted great interests for energy storage devices due to the characteristics of high power density, excellent reversibility, long cycling life, short charge time, and high safety in comparison with batteries [1–3]. They have been considered as the promising high-power sources in electric vehicles, fuel cells, cellular phones, personal digital assistants, telecommunication systems [1, 3, 4], etc. So far, there are two different types of supercapacitors based on the charge storage mechanisms. Type I supercapacitors are electrochemical double-layer capacitors, and type II supercapacitors are known as redox supercapacitors. On the basis of the two types of supercapacitors, an asymmetric supercapacitor has been developed as the new trend in electrochemical capacitors [5]. In such supercapacitor, one electrode stores charge through a reversible nonfaradic process of ionic adsorption/desorption on the activated carbon surface, while the other electrode undergoes a reversible faradic reaction of electroactive materials [6, 7].

To make full use of good performance of supercapacitors, many research activities have focused on the development of new electrode materials, such as transition metal oxides (e.g., RuO_2, IrO_2, MnO_2, NiO, V_2O_5, etc.) and conducting polymers (e.g., PANi, PPy, etc.). Recently, some lithium-ion insertion materials have been of particular interest. For example, $Li_2Ti_3O_7$, $Li_4Ti_5O_{12}$, $LiNi_{0.8}Co_{0.2}O_2$, and $LiCoO_2$ have been used as the electrode materials of asymmetric supercapacitors in organic electrolyte [8–11] and $LiMn_2O_4$, $LiCoO_2$, and $LiNi_{1/3}Co_{1/3}Mn_{1/3}O_2$ used in aqueous solution [12–15]. Among all of the lithium-ion insertion materials, lithium manganese oxides, especially those with spinel structure type, are of high fundamental and technological interest due to their low cost and low toxicity, and they are the most promising electrode materials [16, 17]. $Li_4Mn_5O_{12}$, for example, is a promising electrode material, where all the manganese ions are tetravalent, and lithium ions occupy the 8a tetrahedral positions, whereas the excess of lithium ions with 0.33 and manganese ions reside simultaneously in the 16d octahedral positions, whose formula can be expressed as $Li[Li_{0.33}Mn_{1.67}]O_4$ [18]. It has a 3D interstitial space for the transportation of lithium ions and a good reversibility due to the absence of Mn^{3+} ions with Jahn–Teller effect [19, 20].

Y. Zhao · X. Xu · Q. Lai (✉) · Y. Hao · L. Wang · Z. Lin
College of Chemistry, Sichuan University,
Chengdu 610064, People's Republic of China
e-mail: laiqy5@hotmail.com

There are several approaches to prepare $Li_4Mn_5O_{12}$, such as solid-state reaction [21], melt-impregnation method [22], and so–gel method [23]. The former two preparative methods have common disadvantages: they need higher temperature and longer reaction time. In the case of sol–gel method, it requires lower temperature and shorter reaction time; however, the product particles with homogeneous size and narrow distribution are difficult to be obtained. To overcome the above-mentioned limitations, recently, the emulsion method has received considerable attention [24, 25]. $Li_4Mn_5O_{12}$ nanomaterials prepared by this method may have small particle size, large specific surface area, and much more active reaction sites on the surface, which are in favor of electrolyte dipping and made the electrochemical reaction easy. In this paper, a water-in-oil emulsion method has been used for the first time to synthesize $Li_4Mn_5O_{12}$ nanoparticles with narrow size distribution. It is expected that the sample prepared by the water-in-oil emulsion method will exhibit a good electrochemical capacitance performance.

Experimental

Preparation

To prepare $Li_4Mn_5O_{12}$ nanoparticles, lithium acetate and manganese nitrate were used as the starting materials and were stoichiometrically (Li:Mn=4:5) dissolved in deionized water to form the aqua phase. Cyclohexane was chosen as the oil phase. *n*-hexyl-alcohol and polyoxyethylene (10) octylphenyl ether (OP-10) were adopted as the cosurfactant and surfactant, respectively, which were added into cyclohexane at a volume ratio of 3:2:10. Both aqua and oil phase solutions were mixed at a water-to-oil volume ratio of 1:10 to form a stable transparent pink microemulsion solution by continuously stirring for 8 h. Then, the obtained microemulsion solution was heated at 70 °C until the viscous liquid formed and was further calcined at 450 °C for 4 h.

Characterization

The samples were characterized by X-ray diffraction (XRD). Powder XRD data were collected on a Rigaku D/MAX-rA diffractometer with Cu Kα radiation (λ=0.15418 nm) being operated at 40 kV and 100 mA. The scanning electron microscope (SEM, Hitachi S-450, Japan) was used to observe the grain morphology and particle size.

Electrochemical performance test

The $Li_4Mn_5O_{12}$ electrode was prepared according to the following steps: The mixture containing 70 wt.% of the active material ($Li_4Mn_5O_{12}$), 25 wt.% acetylene black (AB), and 5 wt.% polyvinylidene fluoride (PVDF) was obtained by using *N*-methyl-2-pyrrolidine as the solvent. After the mixture was sufficiently blended, the obtained slurry was dried for 5 h in an infrared light oven and was then pressed onto a stainless steel grid. The activated carbon (AC) electrode was prepared by the same method as stated above; it consisted of 65 wt.% AC, 30 wt.% AB, and 5 wt.% PVDF. Li_2SO_4 solution (1 mol L^{-1}) was used as the electrolyte in this test.

Cyclic voltammetry (CV) measurements were performed by using a three-electrode system, in which $Li_4Mn_5O_{12}$ and platinum were used as the working and counter electrodes, while saturated calomel electrode (SCE) was chosen as the reference electrode. The test was carried out on a TianJin Lanlike Electrochemical Workstation (model LK2005); electrochemical interface was controlled by a computer.

Electrochemical impedance spectroscopy (EIS) measurements were carried out at frequencies from 10 kHz to 0.01 Hz by using an Autolab Electrochemical Workstation, which consists of a three-electrode system with working electrode ($Li_4Mn_5O_{12}$), platinum counter electrode, and SCE reference electrode; electrochemical interface and frequency response analyzer were controlled by a computer.

All the charge/discharge experiments were performed by using Neware Cell Program Control Test System with current density of 100 mA g^{-1} in the range of 0–1.4 V at room temperature, which contains a two-electrode system.

Results and discussion

XRD analysis

Figure 1 shows the XRD pattern of $Li_4Mn_5O_{12}$ powders. Compare the obtained XRD data with JCPDS of $Li_4Mn_5O_{12}$ (no. 46-0810); the 2θ of all the diffraction peaks for the sample is consistent with JCPDS. no. 46-0810. The main diffraction peaks are listed in Table 1. All the diffraction peaks of the sample can be indexed as a face-centered cubic spinel structure with a space group Fd3m. The lattice parameter a is calculated to be 8.165 Å based on the XRD data, which is in good agreement with the literature value of 8.161 Å [26]. The results show that the obtained sample is $Li_4Mn_5O_{12}$. The average particle size of about 15 nm for the sample is estimated according to Scherrer formula based on all the diffraction peaks (the peak broadening effect aroused by the instrument was not taken out). The obtained small size $Li_4Mn_5O_{12}$ powders will be in favor of enhancing their electrochemical performance by increasing the contact area between the particles and electrolyte.

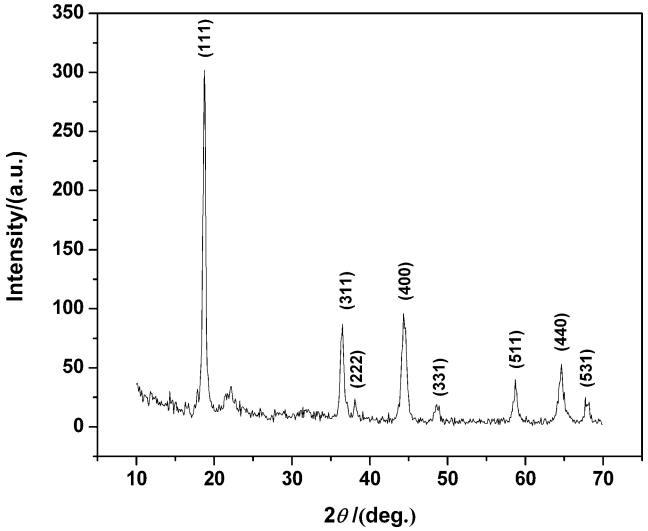

Fig. 1 XRD patterns of the $Li_4Mn_5O_{12}$ powders

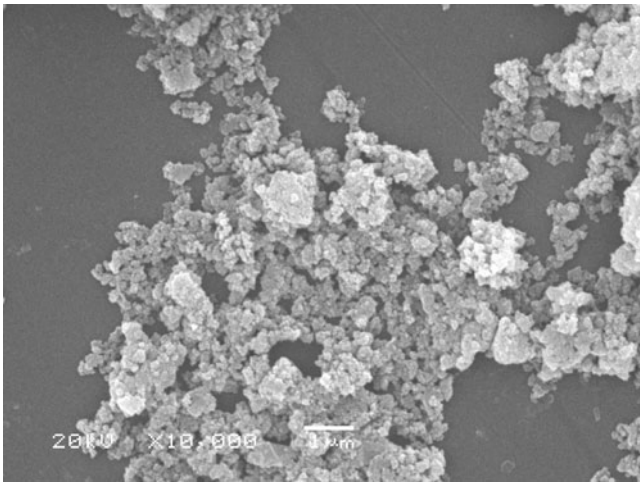

Fig. 2 SEM micrograph of $Li_4Mn_5O_{12}$

SEM analysis

SEM image of $Li_4Mn_5O_{12}$ is shown in Fig. 2. The particles distribute well and exhibit analogous spherical morphology with particle size less than 50 nm.

Electrochemical performance

CV analysis

Figure 3 shows the cyclic voltammograms of $Li_4Mn_5O_{12}$ in 1 mol L^{-1} Li_2SO_4 at different scan rates in the potential range from 0 to 1.4 V. From the CV results, a couple of wide redox peaks located at 0.5 and 1.0 V vs SCE are observed for $Li_4Mn_5O_{12}$ at a scan rate of 2 mV s^{-1}. The single electrode discharge specific capacitance can be estimated from the voltammetric charge surrounded by the CV curve according to the following equation [27, 28]:

$$C = \frac{q_a + |q_c|}{2w\Delta V} \quad (1)$$

where $(q_a+|q_c|)$ is the sum of anodic and cathodic voltammetric charges on positive and negative sweeps, w is the mass of active material, and ΔV is the potential window of CV. Based on Eq. 1, the single electrode discharge specific capacitances are 321, 252, and 169 F g^{-1} at scan rates of 2, 5, and 10 mV s^{-1}, respectively. The specific capacitances decreased with the increase of the scan rate, which is in agreement with the CV curve results. The explanation to this phenomenon is that when the scan rate increases, the intercalation/extraction of lithium ions are limited almost on the crystal surface only, and it is difficult for lithium ions to diffuse into the inner lattice of $Li_4Mn_5O_{12}$ matrix. As a result, the active material is utilized insufficiently, resulting in the specific capacitance decrease with the increase of scan rate. At the same time, the oxidation peaks shift to higher potential while the reduction peaks shift to lower potential gradually. Thus, the potential difference, ΔV, between the oxidation and reduction peaks is increased, which leads to the appearance of electric polarization phenomenon. As the scan rates increase, the electric polarization becomes serious.

As demonstrated above, the conclusion can be drawn that the energy storage mechanism of $Li_4Mn_5O_{12}$ electrode in Li_2SO_4 is as follows:

$$Li_4Mn_5O_{12} + xLi^+ + xe^- \underset{\text{charge}}{\overset{\text{discharge}}{\rightleftharpoons}} Li_{4+x}Mn_5O_{12} \quad (2)$$

During discharge process, lithium ions intercalate into $Li_4Mn_5O_{12}$ structure to form $Li_{4+x}Mn_5O_{12}$, while during charge process, lithium ions are easily extracted from $Li_{4+x}Mn_5O_{12}$ to form $Li_4Mn_5O_{12}$. The whole processes depend on the intercalation/extraction of lithium ions, which are similar to the energy storage mechanism of the lithium ions batteries in organic system.

Table 1 The 2θ of the main diffraction peaks for $Li_4Mn_5O_{12}$

Sample	2θ (°)				
JCPDS. no. 46-0810	18.817	36.483	44.360	58.735	64.536
The obtained $Li_4Mn_5O_{12}$	18.784	36.486	44.365	58.762	64.670

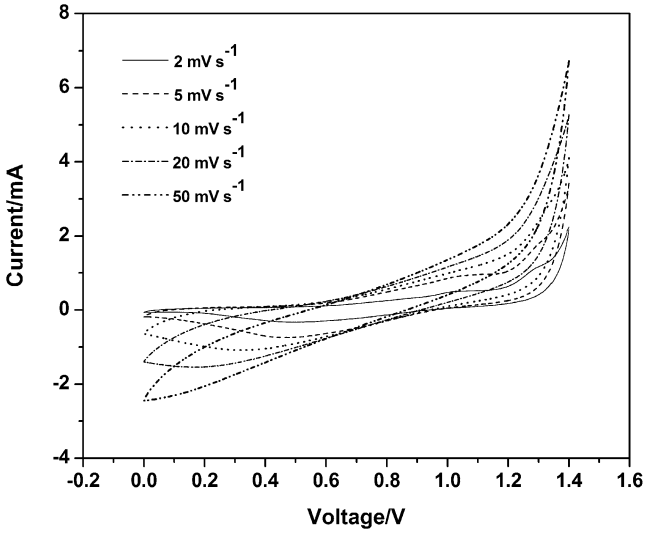

Fig. 3 CV curves of the $Li_4Mn_5O_{12}$ electrode at different scan rates in 1 mol L^{-1} Li_2SO_4

Charge/discharge test at a constant current density

The charge/discharge curves at current density of 100 mA g^{-1} in 1 mol L^{-1} Li_2SO_4 are represented in Fig. 4. It can be seen that the potential is linearly related to time during the charge/discharge process. The slope dV/dt of charge/discharge curves is a constant. The charge and discharge curves exhibit a symmetrical trilateral shape, showing a good electrochemical capacitance performance.

Cycling ability test

Figure 5 shows the cycling ability of $Li_4Mn_5O_{12}$/AC supercapacitor at a current density of 100 mA g^{-1}. After 1,000 cycles, the supercapacitor exhibits a good cycling ability. The coulombic efficiency variation of the supercapacitor with the cycling number is also given in Fig. 5. As can be seen, the coulombic efficiency remained close to 100%, indicating that it has a good cycling performance.

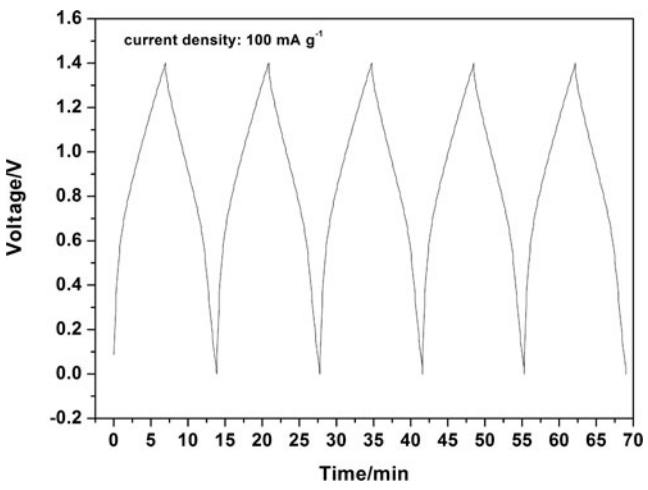

Fig. 4 Charge/discharge curves of the $Li_4Mn_5O_{12}$/AC supercapacitor at 100 mA g^{-1} in 1 mol L^{-1} Li_2SO_4

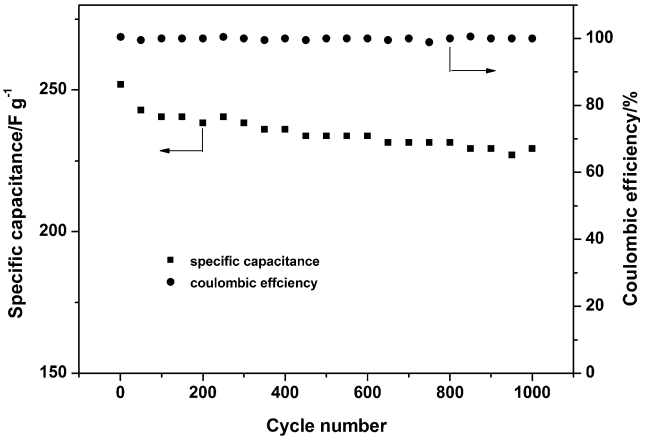

Fig. 5 Cycling ability and coulombic efficiency of $Li_4Mn_5O_{12}$/AC supercapacitor at a current density of 100 mA g^{-1} in 1 mol L^{-1} Li_2SO_4

Electrochemical impedance analysis

The EIS technique was applied to monitor resistance changes in electrolyte/$Li_4Mn_5O_{12}$ interface. As shown in Fig. 6, the EIS plots contain two parts of high- and low-frequency regions. The semicircle in the high-frequency region suggests that there is a charge transfer resistance. The intercept at the real axis of the plot is the internal resistance R_j (5.6 Ω) of the electrode material, suggesting that the material has a good cycling performance. The straight line in the low-frequency region shows that ionic diffusion appears during charge/discharge process. According to the analysis above, it can be known that the energy storage is based on the intercalation of lithium ions which can diffuse not only on the crystal surface but

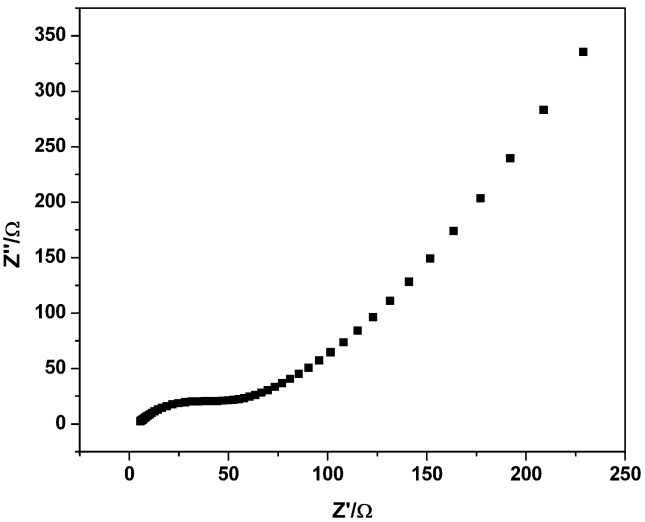

Fig. 6 Electrochemical impedance plots of $Li_4Mn_5O_{12}$ electrode

also into the bulk phase, so is the ionic diffusion in the low-frequency region.

Conclusions

In this study, $Li_4Mn_5O_{12}$ powders with the analogous spherical morphology and average particle size less than 50 nm were prepared by the water-in-oil microemulsion method. The $Li_4Mn_5O_{12}$ and activated carbon were used as electrodes to fabricate $Li_4Mn_5O_{12}$/AC supercapacitor in 1 mol L^{-1} Li_2SO_4. The results of cyclic voltammetry, galvanostatic charge/discharge, and electrochemical impedance spectroscopy measurements proved that this material has a good electrochemical capacitance performance within potential range from 0 to 1.4 V. At a scan rate of 5 mV s^{-1}, it delivered a single electrode specific capacitance of 252 F g^{-1}, and it also showed high coulombic efficiency.

Acknowledgment This work was supported by the National Natural Science Foundation of China (no. 20701029). The authors gratefully thank the help of Xiaoyang Ji and Xinwan Zhang, Analytical and Testing Center at Sichuan University, for the XRD test and SEM morphology.

References

1. Hu CC, Tsou TW (2003) J Power Sources 115:179–186
2. Lee JY, Liang K, An KH, Lee YH (2005) Synth Met 150:153–157
3. Wang CC, Hu CC (2005) Electrochim Acta 50:2573–2581
4. Conway BE (1999) Electrochemical supercapacitors scientific fundamentals and technological applications. Kluwer Academic/Plenum, New York
5. Wang YG, Xia YY (2005) Electrochem Commun 7:1138–1142
6. Pell WG, Conway BE (2004) J Power Sources 136:334–345
7. Wang YG, Wang ZD, Xia YY (2005) Electrochim Acta 50:5641–5646
8. Chen F, Li RG, Hou M, Liu L, Wang R, Deng ZH (2005) Electrochim Acta 51:61–65
9. Amatucci GG, Badway F, Pasquier AD, Zheng T (2001) J Electrochem Soc 148:A930–A939
10. Wang GX, Zhou GM, Yuan RZ, Qu MZ, Zhang BL, Yu ZL (2005) Wu Ji Hua Xue Xue Bao 21:593–597
11. Huang BH, Yang P, Zhang BH, Shi QM (2006) Dian Yuan Ji Shu 30:560–562
12. Wang YG, Xia YY (2006) J Electrochem Soc 153:A450–A454
13. Chen LM, Lai QY, Hao YJ, Huang JH, Ji XY (2008) Ionics 14:441–447
14. Wang YG, Lou JY, Wu W, Wang CC, Xia YY (2007) J Electrochem Soc 154:A228–A234
15. Zhao Y, Wang YY, Lai QY, Chen LM, Hao YJ, Ji XY (2009) Synth Met 159:331–337
16. Tian Y, Chen DR, Jiao XL, Duan YZ (2007) Chem Commun 20:2072–2074
17. Tanaka Y, Zhang QW, Saito F (2003) Powder Technol 132:74–80
18. Takada T, Akiba E, Izumi F, Chakoumakos BC (1997) J Solid State Chem 130:74–80
19. Julien CM, Zaghib K (2004) Electrochim Acta 50:411–416
20. Zhang YC, Wang H, Wang B, Yan H, Ahniyaz A, Yoshimura M (2002) Mater Res Bull 37:1411–1417
21. Julien CM, Massot M (2003) Mat Sci Eng B-Solid 100:69–78
22. Xia YY, Yoshio M (2003) J Power Sources 63:97–102
23. Hao YJ, Wang YY, Lai QY, Zhao Y, Chen LM, Ji XY (2009) J Solid State Electrochem 13:905–912
24. Lu CH, Lin SW (2001) J Power Sources 93:14–19
25. Lu CH, Wang HC (2004) J Eur Ceram Soc 24:717–723
26. Takada T, Hayakawa H, Akiba E, Izumi F, Chakoumakos BC (1997) J Power Sources 68:613–617
27. Hu CC, Wang CC (2002) Electrochem Commun 4:554–559
28. Wang XY, Wang XY, Huang WG, Sebastian PJ, Gamboa S (2005) J Power Sources 140:211–215